
ρ -EOS: Training-free Bidirectional Variable-Length Control for Masked Diffusion LLMs

Jingyi Yang^{1,2} Yuxian Jiang^{1,2} Jing Shao^{1†}

Abstract

Beyond parallel generation and global context modeling, current masked diffusion large language models (masked dLLMs, i.e., LLaDA) suffer from a fundamental limitation: they require a predefined, fixed generation length, which lacks flexibility and forces an inevitable trade-off between output quality and computational efficiency. To address this, we study the denoising dynamics and find that the implicit density (ρ) of end-of-sequence (EOS) tokens serves as a reliable signal of generation sufficiency. In particular, the evolving implicit EOS density during denoising reveals whether the current masked space is excessive or insufficient, thereby guiding the adjustment direction for generation length. Building on this insight, we propose ρ -EOS, a training-free, single-stage strategy that enables bidirectional variable-length generation for masked dLLMs. Unlike prior two-stage approaches—which require separate length adjustment and iterative mask insertion phases while supporting only unidirectional expansion— ρ -EOS achieves bidirectional length adjustment within a unified denoising process by continuously estimating the implicit EOS density: excessively high density triggers MASK token contraction, while insufficient density induces expansion. Extensive experiments on mathematics and code benchmarks demonstrate that ρ -EOS achieves comparable performance while substantially improving inference efficiency and token utilization. Code is available at <https://github.com/yjyddq/rho-EOS>.

guage understanding and generation. Recently, diffusion large language models (dLLMs) (Nie et al., 2025; Khanna et al., 2025; DeepMind, 2025; Song et al., 2025) have emerged as a promising alternative paradigm, attracting increasing attention. In contrast to autoregressive models that generate next-tokens sequentially, dLLMs formulate text generation as a discrete probabilistic denoising process. Starting from a fully masked sequence, dLLMs iteratively unmask MASK tokens in parallel, which enables global context modeling and flexible generation orders.

Despite these advantages, the generation length of dLLMs is fundamentally constrained by their length-rigid generation paradigm. Specifically, inference starts from a fixed number of pre-filled MASK tokens, which strictly determines the final output length. In practice, empirically specifying this length presents a severe dilemma, particularly for long chain reasoning (Lightman et al., 2023; Muennighoff et al., 2025) or tasks that require adaptive switching between short and long thinking modes (hybrid reasoning) (Anthropic, 2025b;a). If the predefined length is too short, the model lacks sufficient token budget to solve complex reasoning tasks. Conversely, adopting a universally long generation length incurs substantial computational overhead, and often results in a low token utilization for tasks with inherently short length, causing significant computational waste. This rigidity stands in sharp contrast to autoregressive models, which can naturally adjust their output length at test time.

To mitigate this limitation, DAEDAL (Li et al., 2025) proposes a two-stage solution that supports only unidirectional expansion through separate initial length adjustment and iterative mask insertion phases. Its first stage iteratively expands an initial short sequence to a coarse target length by checking trailing EOS tokens confidence: if the confidence of EOS tokens is below a threshold, a fixed block of MASK tokens is appended. The second stage then performs iterative mask insertion during denoising to further expand remaining low-confidence regions. While effective, this two-stage pipeline inevitably introduces additional inference latency, making it less suitable for high-throughput or latency-sensitive deployment scenarios. In addition, DAEDAL only supports unidirectional length expansion, lacking the ability to contract the generation length, which becomes problematic when the initial length is overly long, or when earlier

1. Introduction

Autoregressive large language models (Brown et al., 2020; Bai et al., 2023; Touvron et al., 2023; Achiam et al., 2023) have exhibited scaling laws and versatile capabilities in lan-

¹Shanghai Artificial Intelligence Laboratory ²Fudan University.
Correspondence to: Jing Shao <shaojing@pjlab.org.cn>.

Preprint. February 10, 2026.

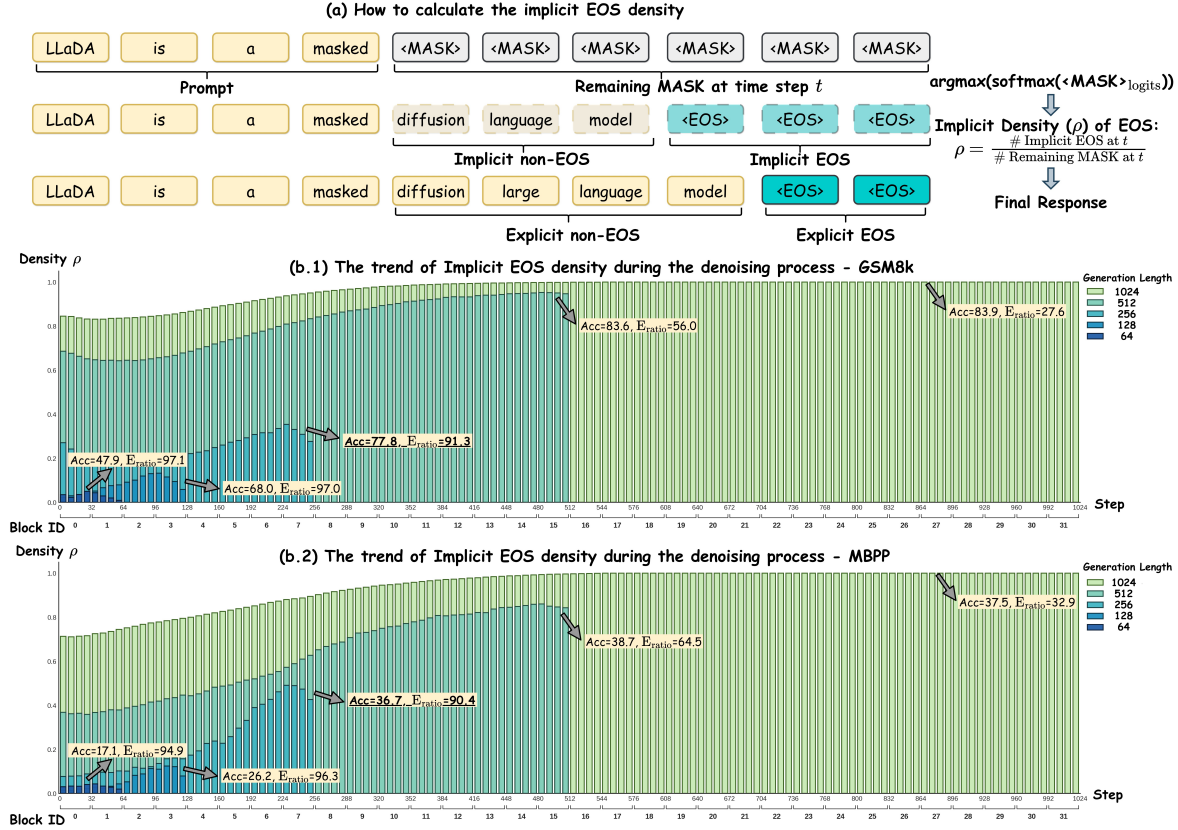


Figure 1. The Evolution Trend of Implicit EOS Density During the Denoising Process. (a) Illustration of the calculation for implicit EOS density. (b.1) Trends of implicit EOS density on GSM8k. (b.2) Trends of implicit EOS density on MBPP.

length expansion decisions are overly aggressive and require later contraction.

To this end, we revisit the denoising dynamics of masked dLLMs and identify an implicit length-indicative signal. As illustrated in Figure 1, under different fixed generation lengths, the implicit EOS density exhibits clearly distinguishable trends throughout the denoising process. When the implicit EOS density is very low, it indicates that the remaining length is insufficient, as the model requires additional space to generate semantic content. In contrast, when the density becomes high, it indicates that the remaining length is excessive, i.e., there is surplus generation capacity. When the length is appropriate—balancing performance and effective token ratio—the density gradually converges to an intermediate equilibrium region. Crucially, this signal emerges naturally during denoising and reflects the model’s internal assessment of length sufficiency. Motivated by this observation, we introduce ρ -EOS, a training-free and bidirectional variable-length denoising strategy. Unlike prior two-stage approaches, ρ -EOS enables denoising and length adaptation jointly within a single stage by monitoring the implicit EOS density.

Extensive experiments demonstrate that ρ -EOS achieves performance comparable to fixed-length baselines and

DAEDAL with significantly improving inference efficiency and token utilization across diverse tasks. Furthermore, compared to DAEDAL, our ρ -EOS supports bidirectional length adjustment, making it more flexible and effective for practical deployment scenarios.

2. Related Work

Diffusion Large Language Models. Given the success of diffusion models in continuous generative modeling, recent work has extended this approach to discrete domains for text generation (Austin et al., 2021a; He et al., 2023; Gong et al., 2022; Lou et al., 2023; Zheng et al., 2024; Sahoo et al., 2024). A prominent paradigm is masked diffusion large language models (dLLMs), which iteratively denoise a masked sequence for bidirectional, parallel generation (Nie et al., 2025; Zhu et al., 2025a;b; Gong et al., 2024; Ye et al., 2025). However, this generation paradigm requires a predefine a fixed generation length, which can lead to either redundant computation when the predefined length is overly long or degraded generation quality when the length budget is insufficient (Li et al., 2025). Another line of dLLMs, known as block diffusion language models (Arriola et al., 2025; Cheng et al., 2025; Liu et al., 2025), naturally supports variable-length generation for adopting a hybrid paradigm

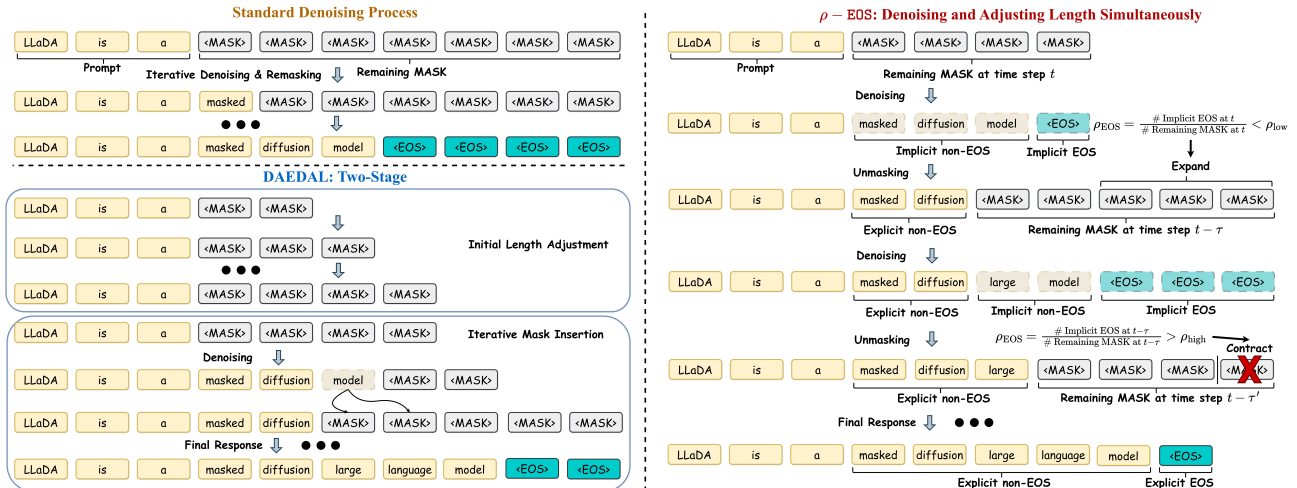


Figure 2. **The Formulation of Implicit and Explicit Concept for Token and Density.** (Upper Left) The standard denoising process of masked diffusion large language models (e.g., LLaDA). (Lower Left) The two stage of DAEDAL. (Right) The bidirectional variable-length denoising process of ρ -EOS.

that divides a sequence into blocks, performs discrete diffusion within each block, and conditions autoregressively on all preceding blocks. In this work, we focus on masked dLLMs and aim to address fixed-length limitation without compromising single-stage denoising paradigm.

Variable-Length Strategies for Masked dLLMs. To alleviate the fixed-length constraint of masked dLLMs, recent works have explored training-based and training-free approaches. For instance, FlexMDMs (Kim et al., 2025) decompose the denoising process into insertion and unmasking steps, learning to predict the number of new MASK tokens to insert before each position. DreamOn (Wu et al., 2025) introduces special control tokens, where EXPAND splits into two MASK tokens to extend the sequence, and DELETE is removed to shorten it. dLLM-Var (Yang et al., 2025b) enables masked dLLMs be able to infer in a block diffusion manner via training the models to accurately predict the EOS token. In contrast, DAEDAL (Li et al., 2025) proposes a training-free alternative that decouples length adjustment from denoising. It first performs length expansion then follow a adaptive denoising. While DAEDAL improves inference efficiency to some extent, its two-stage design potentially introduces additional latency and only supports unidirectional length expansion, which limits flexibility. Moreover, length flexibility also plays a critical role in reinforcement learning (RL) fine-tuning, where diverse reasoning depths and response structures can facilitate exploration (Zhao et al., 2025; Gong et al., 2025; Yang et al., 2025a; Wang et al., 2025). In such settings, RL rollouts and high-throughput deployment are often tightly bottlenecked by inference latency, making multi-stage decoding strategies particularly unfavorable. These considerations further motivate the need for a single-stage, training-free, and bidirectional length control mechanism tailored to masked dLLMs.

3. Methods

3.1. Overview

To address the fixed-length limitation in standard masked diffusion large language models (dLLMs) inference, we introduce ρ -EOS, a training-free, single-stage bidirectional variable-length denoising strategy that enables dLLMs to dynamically adapt their generation length *on the fly* during the denoising process itself, rather than predefining fixed-length or relying on multi-stage heuristics adjustments.

3.2. Implicit Token

We first clarify the concept of **Implicit Token**. At each denoising step, the input \mathbf{x}_t at time step t is forwarded through the model ($p_\theta(\cdot)$) to obtain the logits of input (denote as $\mathbf{x}_t^{\text{logits}}$). These logits are then processed via $\text{argmax}(\text{softmax}(\cdot))$, yielding a prediction of tokens:

$$\mathbf{x}_t^{\text{logits}} = p_\theta(\mathbf{x}_t), \quad (1)$$

$$\hat{\mathbf{x}}_0 = \text{argmax}(\text{softmax}(\mathbf{x}_t^{\text{logits}})), \quad (2)$$

$$\mathbf{x}^{t-\tau} = \text{Remask}(\hat{\mathbf{x}}_0), \quad (3)$$

where $p_\theta(\cdot)$ denotes the model, and $\hat{\mathbf{x}}_0$ represents the model’s prediction of the clean sequence. We refer to $\hat{\mathbf{x}}_0$ as the implicit \mathbf{x}_0 , since it is not immediately committed as final response. Moreover, the tokens in $\hat{\mathbf{x}}_0$ that correspond to the remaining MASK position in \mathbf{x}_t are defined as the **Implicit Tokens** at time step t (i.e., $\{i | \hat{\mathbf{x}}_0^i \wedge (\mathbf{x}_t^i = \text{MASK})\}$). After applying $\text{Remask}(\cdot)$, only a subset of $\hat{\mathbf{x}}_0$ is decoded into **Explicit Tokens**, while the remaining implicit tokens of $\hat{\mathbf{x}}_0$ are remasked to form $\mathbf{x}_{t-\tau}$. This iterative process continues until a fully denoised sequence is obtained, which constitutes the standard inference procedure of masked dLLMs. A schematic illustration is shown in Figure 2.

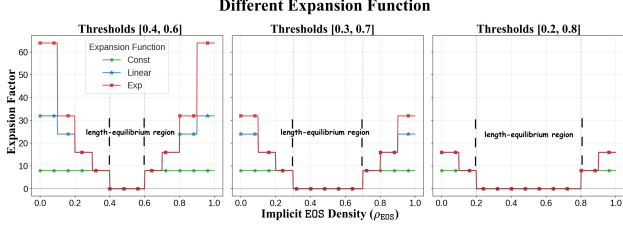


Figure 3. Example of piecewise expansion factor function for constants, linearity, and exponentiation.

3.3. Implicit EOS Density

Based on the notion of implicit tokens, we define **Implicit Density** (ρ) as the ratio between implicit tokens with specific properties and masked tokens at time step t . As depicted at the right panel of Figure 2, implicit token density:

$$\rho = \frac{\# \text{ Implicit Token at } t}{\# \text{ Remaining MASK Token at } t}, \quad (4)$$

where # Implicit Token at t denotes the number of implicit tokens with certain properties at timestep t , and # Remaining MASK Token at t represents the number of remaining MASK tokens in \mathbf{x}_t needed to be denoised. Subsequently, we conclude the implicit EOS density:

$$\rho_{\text{EOS}} = \frac{\# \text{ Implicit EOS Token at } t}{\# \text{ Remaining MASK Token at } t}. \quad (5)$$

3.4. Bidirectional Length Adjustment

As illustrated in Figure 1 (which shows the trend of ρ_{EOS} on GSM8k and MBPP across fixed-length ranging from 64 to 1024), we observe that masked dLLMs implicitly encode length sufficiency information in ρ_{EOS} . When the masked budget is sufficient to complete the response, the model assigns higher probability mass to EOS, resulting in a larger ρ_{EOS} . Conversely, when the available length is insufficient, the model tends to fully utilize the masked space for semantic contents, leading to a persistently low ρ_{EOS} . This behavior indicates that ρ_{EOS} serves as a reliable internal signal for assessing whether the current generation length is appropriate.

Similarly, as demonstrated in Figure 1, when the generation length is excessively long (e.g., 512 or 1024), the ρ_{EOS} converges toward near 1, indicating a waste of capacity. Conversely, when the length is too short (e.g., 64 or 128), the density converges toward 0, signaling insufficient semantic content. This observation suggests that the ideal implicit EOS density does not converge to an extreme value but rather reaches an intermediate **length-sufficiency equilibrium state**, which reflects a suitable length for both quality and efficiency. To operate this criterion robust, we empirically define the **length-equilibrium region** using two thresholds ρ_{low} and ρ_{high} . When $\rho_{\text{EOS}} \in [\rho_{\text{low}}, \rho_{\text{high}}]$,

Algorithm 1 The Inference Process of ρ -EOS

```

1: Input: Prompt  $\mathbf{p}$ , model  $p_\theta$ , initial/max length  $L_{\text{init}}/L_{\text{max}}$ , density thresholds  $[\rho_{\text{low}}, \rho_{\text{high}}]$ , confidence threshold  $\tau_{\text{high}}$ , expansion factor function  $E_{\text{factor}}(\cdot)$ , max length adjustment step  $N$ 
2: Output: clean sequence  $\mathbf{x}$ 
3:  $L_{\text{cur}} \leftarrow L_{\text{init}}, n \leftarrow 0$ 
4:  $\mathbf{x}^t \leftarrow \underbrace{[\mathbf{p}, \text{MASK}, \dots, \text{MASK}]}_{L_{\text{init}}}$   $\triangleright$  Initialize sequence
5: while ContainsMask( $\mathbf{x}_t$ ) do
6:    $\mathbf{x}_t^{\text{logits}} \leftarrow p_\theta(\mathbf{x}_t)$ 
7:    $\rho_{\text{EOS}} \leftarrow \text{ImplicitEOSDensity}(\mathbf{x}_t^{\text{logits}})$ 
8:    $\mathbf{x}_t^{\text{conf}}, \hat{\mathbf{x}}_0 \leftarrow \text{Decode}(\mathbf{x}_t^{\text{logits}})$ 
9:   for  $i \in \{(\mathbf{x}_t^i = \text{MASK}) \wedge (\mathbf{x}_t^{\text{conf}, i} > \tau_{\text{high}})\}$  do
10:     $\mathbf{x}_{t-\tau}^i \leftarrow \hat{\mathbf{x}}_0^i$ 
11:   end for
12:   if  $0 < L_{\text{cur}} < L_{\text{max}}$  and  $n < N$  then
13:     if  $\rho_{\text{EOS}} \in [\rho_{\text{low}}, \rho_{\text{high}}]$  then
14:        $\mathbf{x}_t, L_{\text{cur}} \leftarrow \mathbf{x}_{t-\tau}, L_{\text{cur}}$   $\triangleright$  Hold  $L_{\text{cur}}$ 
15:     else if  $\rho_{\text{EOS}} < \rho_{\text{low}}$  then  $\triangleright$  Expand  $L_{\text{cur}}$ 
16:        $\mathbf{x}_{t-\tau} \leftarrow \mathbf{x}_{t-\tau} \oplus \underbrace{[\text{MASK}, \dots, \text{MASK}]}_{E_{\text{factor}}(\rho_{\text{EOS}})}$ 
17:        $L_{\text{cur}} \leftarrow L_{\text{cur}} + E_{\text{factor}}(\rho_{\text{EOS}})$ 
18:     else  $\triangleright$  Contract  $L_{\text{cur}}$ 
19:        $\mathbf{x}_{t-\tau} \leftarrow \mathbf{x}_{t-\tau}^{0: (|\mathbf{x}| - E_{\text{factor}}(\rho_{\text{EOS}}))}$ 
20:        $L_{\text{cur}} \leftarrow L_{\text{cur}} - E_{\text{factor}}(\rho_{\text{EOS}})$ 
21:     end if
22:   end if
23:    $n \leftarrow n + 1$ 
24: end while
25: return  $\mathbf{x}$ 

```

the model suspends length modification and focuses solely on denoising, enabling stable bidirectional control without oscillatory behavior. When $\rho_{\text{EOS}} < \rho_{\text{low}}$, the remaining masked space is insufficient and length expansion is triggered via MASK insertion. Conversely, when $\rho_{\text{EOS}} > \rho_{\text{high}}$, the model indicates surplus generation capacity and the sequence is contracted by removing partial trailing MASK.

Formally, the length adjustment is defined as:

$$\mathbf{x} = \begin{cases} \mathbf{x} \leftarrow \mathbf{x} \oplus \underbrace{[\text{MASK}, \dots, \text{MASK}]}_{E_{\text{factor}}(\rho_{\text{EOS}})} & \text{if } \rho_{\text{EOS}} < \rho_{\text{low}} \\ \mathbf{x} \leftarrow \mathbf{x}^{0: (|\mathbf{x}| - E_{\text{factor}}(\rho_{\text{EOS}}))} & \text{else if } \rho_{\text{EOS}} > \rho_{\text{high}} \\ \mathbf{x} & \text{otherwise} \end{cases} \quad (6)$$

with the update to current generation length L_{cur} :

$$L_{\text{cur}} = \begin{cases} L_{\text{cur}} + E_{\text{factor}}(\rho_{\text{EOS}}) & \text{if } \rho_{\text{EOS}} < \rho_{\text{low}} \\ L_{\text{cur}} - E_{\text{factor}}(\rho_{\text{EOS}}) & \text{else if } \rho_{\text{EOS}} > \rho_{\text{high}} \\ L_{\text{cur}} & \text{otherwise} \end{cases} \quad (7)$$

Table 1. Main Results on LLaDA-Instruct-8B across Four Benchmarks. We compare the ρ -EOS performance against DAEDAL and various baseline configurations. *Acc* denotes accuracy, E_{token} is the average effective tokens (the response length excluding trailing padding), N_{token} is the average total tokens, and E_{ratio} is the effective token ratio. T_{runtime} represents the runtime spent on the evaluation (in seconds). The best configuration for the baseline is highlighted in orange. DAEDAL is highlighted in blue, and ρ -EOS is highlighted in red. Under the ρ -EOS setting, Sym and Asym denote the symmetric and asymmetric lower-upper threshold centered around 0.5. The best results are bold, and the second-best results are underlined.

| Benchmark | Metric | Fixed-Length Denoising (Baseline) | | | | | DAEDAL | ρ -EOS | ρ -EOS | |
|------------|----------------------|-----------------------------------|-------|-------|-------|-------------|-------------|--------------|--------------|--------------|
| | | 64 | 128 | 256 | 512 | 1024 | 2048 | 64 | 64 Sym | 64 Asym |
| GSM8K | <i>Acc</i> | 47.9 | 68.0 | 77.8 | 83.6 | 83.9 | 82.7 | 84.6 | 81.8 | <u>84.2</u> |
| | E_{token} | 62.1 | 124.1 | 233.7 | 286.8 | 282.9 | 297.3 | 246.0 | 198.4 | 252.5 |
| | N_{token} | 64 | 128 | 256 | 512 | 1024 | 2048 | 331.0 | 231.8 | 361.0 |
| | E_{ratio} | 97.1% | 97.0% | 91.3% | 56.0% | 27.6% | 14.5% | <u>74.5%</u> | 85.6% | 70.0% |
| | T_{runtime} | 174 | 360 | 860 | 2458 | 8238 | 30305 | 1090 | 645 | <u>823</u> |
| | | | | | | | | | | |
| MATH500 | <i>Acc</i> | 24.0 | 29.0 | 35.4 | 38.4 | <u>40.4</u> | 40.0 | 40.0 | 37.0 | 40.6 |
| | E_{token} | 61.7 | 123.3 | 244.7 | 423.9 | 585.8 | 706.5 | 464.6 | 428.8 | 558.7 |
| | N_{token} | 64 | 128 | 256 | 512 | 1024 | 2048 | 618.3 | 486.3 | 682.2 |
| | E_{ratio} | 96.4% | 96.3% | 95.6% | 82.8% | 57.2% | 34.5% | 75.2% | 88.2% | <u>81.9%</u> |
| | T_{runtime} | 98 | 208 | 462 | 1202 | 3663 | 12764 | 2207 | 1398 | <u>1968</u> |
| | | | | | | | | | | |
| MBPP | <i>Acc</i> | 21.0 | 28.8 | 36.7 | 38.7 | 37.5 | 38.8 | 39.4 | <u>39.6</u> | 40.6 |
| | E_{token} | 61 | 122 | 232 | 331 | 335 | 336 | 308.4 | 324.0 | 335.9 |
| | N_{token} | 64 | 128 | 256 | 512 | 1024 | 2048 | 558.3 | 507.4 | 594.4 |
| | E_{ratio} | 94.9% | 95.5% | 90.4% | 64.5% | 32.9% | 16.3% | 55.2% | 63.9% | <u>55.5%</u> |
| | T_{runtime} | 176 | 332 | 713 | 1728 | 4760 | 15172 | 3551 | <u>2031</u> | 2030 |
| | | | | | | | | | | |
| HUMAN EVAL | <i>Acc</i> | 17.1 | 26.2 | 36.6 | 45.1 | 45.1 | 48.2 | <u>44.5</u> | 43.3 | 43.9 |
| | E_{token} | 59.6 | 125 | 247.3 | 462 | 631.1 | 691.1 | 494.7 | 570.4 | 643.1 |
| | N_{token} | 64 | 128 | 256 | 512 | 1024 | 2048 | 813.0 | 654.0 | 769.9 |
| | E_{ratio} | 93.2% | 97.7% | 96.6% | 90.2% | 61.6% | 33.8% | 64.8% | 88.4% | <u>83.5%</u> |
| | T_{runtime} | 111 | 230 | 543 | 1474 | 4569 | 16046 | 1283 | 580 | <u>593</u> |
| | | | | | | | | | | |

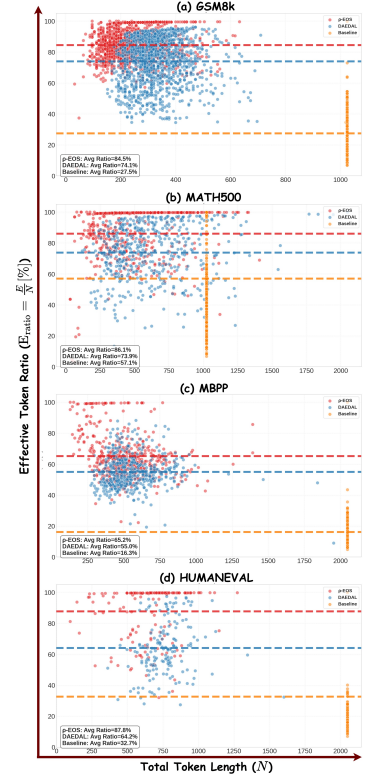


Figure 4. E_{ratio} per sample.

Beyond above, we further investigate how aggressively the adjustment should be performed through different **expansion factor functions** $E_{\text{factor}}(\cdot)$. DAEDAL (Li et al., 2025) adopts a constant expansion factor, a design that is simple and stable but lead to multiple adjustment iterations when the initial length is severely mismatched. Motivated by Figure 1, we additionally consider linear and exponential designs, as depicted in Figure 3. The piecewise linear function scales the adjustment magnitude proportionally to the distance between ρ_{EOS} and the length-equilibrium region boundaries. The piecewise exponential function further amplifies this effect when ρ_{EOS} is extremely low or high, enabling more aggressive expansion or contraction. The key motivation is to rapidly drive the generation into the stable ρ_{EOS} region, so that the model can enter the pure denoising phase early without repeatedly interleaving length adjustment steps. Compared to unidirectional expansion, bidirectional control improves flexibility and token utilization. As illustrated in Figure 2, if the length becomes overly aggressive after expansion, the proposed mechanism can actively contract the sequence, leading to more efficient and stable generation.

3.5. One-Stage Bidirectional Variable-Length Denoising

Overall, by integrating implicit EOS density estimation with bidirectional length adjustment, ρ -EOS realizes **training-**

free and bidirectional variable-length generation in a fully unified, single-stage denoising process, i.e., jointly performs unmasking (decoding) and length adjustment. At each denoising step, the model $p_{\theta}(\cdot)$ performs once forward pass on the \mathbf{x}_t to obtain $\mathbf{x}_t^{\text{logits}}$ and the implicit prediction $\hat{\mathbf{x}}_0$ (Equation 3). After applying the $\text{Remask}(\cdot)$ operation to produce $\mathbf{x}_{t-\tau} = \text{Remask}(\hat{\mathbf{x}}_0)$, we compute ρ_{EOS} according to Equation 5 and adjust the current sequence length using the bidirectional strategy in Equations 6 and 7. This step-level denoising process is repeated until entire denoising completes. By coupling denoising and length adjustment within a single inference loop, ρ -EOS enables dynamic expansion when additional reasoning space is needed and contraction when redundancy is detected, without introducing extra stages. Algorithm 1 provides a detailed description of the full procedure.

4. Experiments

4.1. Experimental Setups

Implementation Details. We follow the experimental settings of DAEDAL (Li et al., 2025) to ensure fairness and reproducibility. All experiments are conducted under the standard generation, without employing additional acceleration or caching mechanisms, and the batch size is set to 8. To mitigate randomness from a single evaluation run,

Table 2. Main Results on LLaDA-1.5-8B across Four Benchmarks. We compare the ρ -EOS performance against DAEDAL and various baseline configurations. Acc denotes accuracy, E_{token} is the average effective tokens (the response length excluding trailing padding), N_{token} is the average total tokens, and E_{ratio} is the effective token ratio. $T_{runtime}$ represents the runtime spent on the evaluation (in seconds). The best configuration for the baseline is highlighted in orange. DAEDAL is highlighted in blue, and ρ -EOS is highlighted in red. Under the ρ -EOS setting, Sym and Asym denote the symmetric and asymmetric lower-upper threshold centered around 0.5. The best results are bold, and the second-best results are underlined.

| Benchmark | Metric | Fixed-Length Denoising (Baseline) | | | | | | DAEDAL | ρ -EOS | ρ -EOS |
|-----------|---------------|-----------------------------------|-------|-------|-------|-------------|-------|--------------|--------------|--------------|
| | | 64 | 128 | 256 | 512 | 1024 | 2048 | 64 | 64 Sym | 64 Asym |
| GSM8K | Acc | 49.9 | 71.2 | 80.5 | 83.6 | 83.9 | 84.2 | 85.1 | 83.3 | <u>84.5</u> |
| | E_{token} | 62.4 | 124.8 | 236.7 | 292.6 | 287 | 293.9 | 254.7 | 214.5 | 231.6 |
| | N_{token} | 64 | 128 | 256 | 512 | 1024 | 2048 | 348.3 | 254.3 | 362.4 |
| | E_{ratio} | 97.1% | 97.0% | 91.2% | 56.0% | 27.7% | 14.4% | <u>72.9%</u> | 84.4% | 63.9% |
| | $T_{runtime}$ | 149 | 335 | 844 | 2488 | 8450 | 30875 | 1056 | 721 | <u>990</u> |
| | | | | | | | | | | |
| MATH500 | Acc | 22.8 | 30.2 | 35.2 | 39.2 | 42.8 | 39.4 | <u>42.6</u> | 38.2 | 41.0 |
| | E_{token} | 62.1 | 124.8 | 246.5 | 428.6 | 583.5 | 713.7 | 489.1 | 339.5 | 583.4 |
| | N_{token} | 64 | 128 | 256 | 512 | 1024 | 2048 | 662.6 | 373.1 | 711.3 |
| | E_{ratio} | 97.0% | 97.5% | 96.3% | 83.7% | 57.0% | 34.9% | 73.8% | 91.0% | <u>82.0%</u> |
| | $T_{runtime}$ | 97 | 192 | 444 | 1177 | 3616 | 12610 | 2460 | 850 | 637 |
| | | | | | | | | | | |
| MBPP | Acc | 21.2 | 30.4 | 39.2 | 38.8 | <u>39.4</u> | 39.4 | 38.2 | 40.8 | 40.8 |
| | E_{token} | 60.9 | 123.7 | 238.2 | 347.3 | 343.5 | 356.2 | 321.8 | 336.1 | 334.1 |
| | N_{token} | 64 | 128 | 256 | 512 | 1024 | 2048 | 587.1 | 535.6 | 540.8 |
| | E_{ratio} | 95.1% | 96.6% | 93.0% | 67.8% | 33.6% | 17.4% | 54.8% | 62.8% | <u>61.8%</u> |
| | $T_{runtime}$ | 156 | 313 | 690 | 1689 | 4688 | 14895 | 4124 | <u>3001</u> | 2565 |
| | | | | | | | | | | |
| HUMANEVAL | Acc | 17.6 | 20.7 | 38.4 | 45.1 | 49.4 | 48.8 | 43.9 | <u>44.5</u> | <u>44.5</u> |
| | E_{token} | 60.3 | 124.9 | 251.7 | 473.8 | 672.1 | 761.6 | 523 | 460.8 | 686.6 |
| | N_{token} | 64 | 128 | 256 | 512 | 1024 | 2048 | 806.4 | 509.7 | 809.5 |
| | E_{ratio} | 94.2% | 97.5% | 98.3% | 92.5% | 65.6% | 37.2% | 64.4% | 90.4% | <u>84.8%</u> |
| | $T_{runtime}$ | 47 | 78 | 162 | 406 | 1212 | 4187 | 743 | 433 | <u>647</u> |
| | | | | | | | | | | |

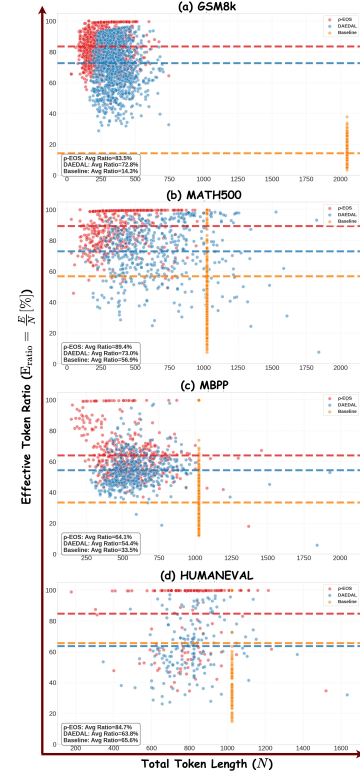


Figure 5. E_{ratio} per sample.

each experiment is repeated three times, and we report the averaged results.

Benchmarks and Metrics. To comprehensively evaluate the effectiveness of ρ -EOS, we conduct experiments on four benchmarks covering mathematics and code task. For mathematics, we evaluate on GSM8K (Cobbe et al., 2021), which consists of grade-school math word problems, and MATH500 (Lightman et al., 2023), a more challenging benchmark composed of competition-level mathematical problems. Accuracy is adopted as the performance metric. For code generation, we employ MBPP (Austin et al., 2021b), which focuses on entry-level Python programming tasks, and HumanEval (Chen et al., 2021), a more challenging handwritten benchmark for program synthesis. We report the standard pass@1 (accuracy) metric to assess functional correctness. In addition to accuracy (Acc), we introduce four efficiency-related metrics: the total number of generated tokens (N_{token}), the number of effective tokens after removing trailing EOS padding (E_{token}), the effective token ratio ($E_{ratio} = \frac{E_{token}}{N_{token}}$), and the evaluation runtime ($T_{runtime}$, in seconds).

4.2. Main Results

We report the main results in Table 1 and Table 2, comparing fixed-length baselines, DAEDAL, and our proposed ρ -EOS. The fixed-length baselines are evaluated under six

predefined generation lengths ranging from 64 to 2048. Both DAEDAL and ρ -EOS start from the same short initial length, $L_{init} = 64$, ensuring a fair comparison.

Performance of ρ -EOS with an initial length of 64. As shown in Table 1 and Table 2, ρ -EOS achieves performance comparable to DAEDAL and the best-performing fixed-length baselines across most benchmarks. Under MATH500 and MBPP in Table 1, the performance of ρ -EOS with $L_{init} = 64$ Asym suppresses both of them, and ρ -EOS consistently demonstrates substantially higher efficiency. Under MBPP and HUMANEVAL in Table 2, the performance of ρ -EOS with $L_{init} = 64$ Asym suppresses DAEDAL, and ρ -EOS consistently outperforms DAEDAL and best-performance baseline on efficiency. More importantly, both the effective token ratio (E_{ratio}) and evaluation runtime ($T_{runtime}$) significantly outperform DAEDAL and the strongest fixed-length baselines on nearly all tasks. By simultaneously performing length adjustment and denoising within a unified diffusion process, ρ -EOS adapts task-dependent generation lengths on the fly, achieving competitive accuracy at a substantially lower computational cost.

ρ -EOS significantly improves effective token ratio and evaluation speed. For best-performance fixed-length baselines, the price for this performance comes at the cost of sharply increased evaluation runtime ($T_{runtime}$) and significantly reduced effective token ratio (E_{ratio}). In particu-

Table 3. **Variou-Initial Length Results on LLaDA-Instruct-8B and LLaDA-1.5-8B.** We compare ρ -EOS at various-initial lengths (128 to 1024) against DAEDAL. The best results are bold, and the second-best results are underlined.

| Benchmark | Metric | LLaDA Variou-Init-Length | | | | | | | | | | LLaDA1.5 Variou-Init-Length | | | | | | | | | |
|-----------|----------------------|--------------------------|-------------|--------|-------------|--------|-------------|--------|-------------|---------------|---------------|-----------------------------|-------------|--------|-------------|--------|-------------|--------|-------------|---------------|---------------|
| | | 128 | | 256 | | 512 | | 1024 | | Average | | 128 | | 256 | | 512 | | 1024 | | Average | |
| | | DAEDAL | ρ -EOS | DAEDAL | ρ -EOS | DAEDAL | ρ -EOS | DAEDAL | ρ -EOS | DAEDAL | ρ -EOS | DAEDAL | ρ -EOS | DAEDAL | ρ -EOS | DAEDAL | ρ -EOS | DAEDAL | ρ -EOS | DAEDAL | ρ -EOS |
| GSM8K | Acc | 84.6 | 84.6 | 84.0 | 83.7 | 85.3 | 84.4 | 84.8 | 84.8 | 84.7 | <u>84.4</u> | 85.1 | 85.2 | 85.0 | 83.8 | 84.2 | 84.3 | 85.9 | 84.9 | 85.1 | <u>84.5</u> |
| | E_{token} | 246.3 | 231.8 | 250.2 | 284.7 | 286.8 | 288.6 | 281.3 | 282.6 | 266.2 | 271.9 | 254.7 | 257.8 | 256.9 | 261.0 | 275.7 | 293.7 | 284.0 | 292.5 | 267.8 | 276.3 |
| | N_{token} | 330.8 | 313.0 | 341.1 | 336.4 | 530.0 | 438.6 | 1040.0 | 666.8 | 560.5 | 438.7 | 349.3 | 370.5 | 356.4 | 321.0 | 531.4 | 474.2 | 1040.0 | 398.0 | 569.3 | 390.9 |
| | E_{ratio} | 74.5% | 74.1% | 73.4% | 84.6% | 50.9% | 65.8% | 27.0% | 42.4% | <u>56.5%</u> | 66.7% | 72.9% | 69.6% | 72.1% | 81.3% | 51.9% | 61.9% | 27.3% | 73.5% | <u>56.1%</u> | 71.6% |
| | T_{runtime} | 1035 | 835 | 1014 | 834 | 1090 | 1044 | 5656 | 1809 | <u>2199.0</u> | 1131.0 | 1093 | 990 | 1008 | 638 | 1223 | 1122 | 5476 | 1281 | <u>2200.0</u> | 1007.8 |
| MATH500 | Acc | 42.6 | 40.0 | 43.2 | 40.4 | 41.8 | 42.8 | 41.6 | 39.8 | 42.3 | <u>40.8</u> | 42.6 | 40.6 | 43.0 | 41.2 | 41.4 | 42.0 | 40.0 | 40.6 | 41.8 | <u>41.1</u> |
| | E_{token} | 464.6 | 410.8 | 465.7 | 492.2 | 479.0 | 556.6 | 541.4 | 588.4 | 487.7 | 512.0 | 489.1 | 528.1 | 490.0 | 559.2 | 499.4 | 586.7 | 534.3 | 602.3 | 503.2 | 569.1 |
| | N_{token} | 618.4 | 480.8 | 621.0 | 549.2 | 686.8 | 642.0 | 1058.8 | 874.1 | 746.3 | 636.5 | 662.6 | 624.1 | 664.2 | 664.3 | 717.7 | 692.9 | 1064.9 | 792.1 | 777.4 | 693.4 |
| | E_{ratio} | 75.1% | 89.2% | 75.0% | 89.5% | 69.7% | 86.7% | 51.1% | 67.3% | <u>67.7%</u> | 83.2% | 73.8% | 84.6% | 73.8% | 84.2% | 69.6% | 84.7% | 50.2% | 76.0% | <u>66.9%</u> | 82.4% |
| | T_{runtime} | 2199 | 1062 | 2175 | 1543 | 2096 | 1980 | 6543 | 1938 | <u>3253.3</u> | 1630.8 | 2447 | 1805 | 2423 | 1912 | 2345 | 2074 | 2315 | 2199 | <u>2382.5</u> | 1997.5 |
| MBPP | Acc | 39.4 | 39.0 | 39.4 | 40.0 | 38.8 | 39.4 | 37.8 | 38.6 | 38.8 | <u>39.3</u> | 38.2 | 41.8 | 38.2 | 41.4 | 37.8 | 39.0 | 40.0 | 40.4 | 38.6 | <u>40.7</u> |
| | E_{token} | 308.4 | 341.6 | 308.4 | 344.0 | 313.0 | 342.5 | 324.7 | 345.0 | 313.6 | 343.3 | 321.8 | 345.1 | 321.8 | 350.2 | 325.4 | 362.1 | 331.5 | 350.7 | 325.1 | 352.0 |
| | N_{token} | 558.3 | 605.1 | 558.3 | 611.6 | 604.6 | 638.3 | 1046.7 | 773.5 | 692.0 | 657.1 | 587.1 | 556.5 | 587.1 | 497.7 | 621.4 | 662.8 | 1046.8 | 943.6 | 710.6 | 665.2 |
| | E_{ratio} | 55.2% | 56.5% | 55.2% | 56.3% | 51.8% | 53.6% | 31.0% | 44.6% | <u>48.3%</u> | 52.8% | 54.8% | 62.0% | 54.8% | 70.4% | 52.4% | 54.6% | 31.7% | 37.2% | <u>48.4%</u> | 56.1% |
| | T_{runtime} | 3518 | 2836 | 3462 | 2169 | 3303 | 2389 | 5674 | 2558 | <u>3989.3</u> | 2396.0 | 4102 | 2824 | 4060 | 1853 | 3907 | 2585 | 4471 | 2501 | <u>4133.0</u> | 2440.8 |
| HUMANEVAL | Acc | 48.2 | 48.8 | 48.2 | 47.0 | 48.2 | 45.1 | 47.0 | 47.6 | 47.9 | <u>47.1</u> | 43.9 | 47.6 | 43.9 | 47.0 | 43.9 | 48.2 | 43.9 | 49.4 | 43.9 | <u>48.1</u> |
| | E_{token} | 497.5 | 618.0 | 497.5 | 613.0 | 497.3 | 613.7 | 540.0 | 638.8 | 508.1 | 620.9 | 519.2 | 634.7 | 519.2 | 654.5 | 518.8 | 623.6 | 528.4 | 677.6 | 521.4 | 647.6 |
| | N_{token} | 769.5 | 693.5 | 769.5 | 698.7 | 772.4 | 717.8 | 1046.9 | 927.9 | 839.6 | 759.5 | 806.4 | 734.9 | 806.4 | 743.0 | 808.4 | 692.2 | 1049.4 | 951.5 | 867.7 | 780.4 |
| | E_{ratio} | 64.7% | 89.1% | 64.7% | 87.7% | 64.4% | 85.5% | 51.6% | 68.8% | <u>61.4%</u> | 82.8% | 64.4% | 86.4% | 64.4% | 88.1% | 64.2% | 90.1% | 50.4% | 71.2% | <u>60.9%</u> | 84.0% |
| | T_{runtime} | 746 | 528 | 789 | 542 | 725 | 548 | 1644 | 618 | <u>976.0</u> | 559.0 | 786 | 590 | 730 | 593 | 705 | 623 | 798 | 606 | <u>754.8</u> | 603.0 |

Table 4. **Ablation on ρ_{high} and ρ_{low} .** Ablations are conducted on GSM8k with LLaDA-Instruct-8B, and $L_{\text{init}} = 64$. The threshold of density (ρ) ranging from 0 to 1. We highlight our best-performance Asym setting ($[\rho_{\text{low}} = 0.4, \rho_{\text{high}} = 0.8]$) in red.

| Metric | Density Threshold $[\rho_{\text{low}}, \rho_{\text{high}}]$ | | | |
|----------------------|---|------------|------------|--------------|
| | [0.2, 0.8] | [0.3, 0.7] | [0.4, 0.6] | [0.4, 0.8] |
| Acc | 81.8 | 81.7 | 81.7 | 84.2 |
| E_{token} | 198.4 | 210.5 | 218.4 | 252.5 |
| N_{token} | 231.8 | 251.2 | 267.5 | 361.0 |
| E_{ratio} | 85.6% | 83.8% | 81.6% | 70.0% |
| T_{runtime} | 645 | 722 | 845 | 823 |

lar, configurations such as (MBPP, 2048), (HUMANEVAL, 2048) in Table 1, and (GSM8k, 2048) in Table 2 exhibit extremely low E_{ratio} , accompanied by a dramatic increase in T_{runtime} . While DAEDAL partially alleviates this inefficiency, ρ -EOS further improves computational efficiency. By enabling bidirectional length adjustment, ρ -EOS consistently achieves higher E_{ratio} than both DAEDAL and the best-performing fixed-length baselines at comparable accuracy levels. This reduces unnecessary bidirectional attention over excessively long sequences and minimizes wasted computation on redundant padding tokens. To provide a more fine-grained view, Figure 4 and Figure 5 visualize the per-sample distribution of total generation lengths (N_{token}) and the corresponding effective token ratio E_{ratio} . Across all four benchmarks, a substantial portion of samples generated by ρ -EOS achieve an E_{ratio} close to 100%, approaching the efficiency of autoregressive counterparts. Such behavior is rarely observed in DAEDAL or fixed-length baselines, further illustrating the superior efficiency of variable-length denoising with bidirectional control.

4.3. Robustness and Ablation Studies

Robustness to the initial length. Table 3 demonstrates that ρ -EOS exhibits strong robustness to the choice of the initial generation length. When varying L_{init} from 128 to 1024, ρ -EOS maintains remarkably stable accuracy, while consistently achieving higher effective token ratio and sig-

Table 5. **Ablation on Expansion Factor Function.** Ablations are conducted on GSM8K with LLaDA-Instruct-8B, $L_{\text{init}} = 64$ and $[\rho_{\text{low}} = 0.4, \rho_{\text{high}} = 0.6]$. **Step** is the average adjustment steps.

| Metric | Expansion Factor Function $E_{\text{factor}}(\cdot)$ | | | |
|----------------------|--|---------------------------|----------------------------|-------------------------|
| | Baseline ₂₅₆ | $E_{\text{const}}(\cdot)$ | $E_{\text{linear}}(\cdot)$ | $E_{\text{exp}}(\cdot)$ |
| Acc | 77.8 | 79.8 | 80.9 | 81.7 |
| E_{token} | 233.7 | 183.4 | 208.0 | 218.4 |
| N_{token} | 256 | 213.3 | 251.0 | 267.5 |
| E_{ratio} | 91.3% | 86.0% | 82.9% | 81.6% |
| T_{runtime} | 860 | 589 | 757 | 845 |
| Step | - | 61.0 | 54.8 | 52.4 |

nificantly lower runtime compared to DAEDAL across all benchmarks. In contrast, DAEDAL shows a clear sensitivity to the initial length on E_{ratio} and T_{runtime} aspects. The robustness of stems from its **bidirectional length adjustment mechanism driven by implicit EOS density**. Rather than committing to a fixed or unidirectional expansion strategy, ρ -EOS dynamically contracts or expands the sequence based on whether the current length is over- or under-sufficient. As a result, even when initialized with an aggressive or conservative length, the model can rapidly converge toward a task-adaptive length regime. This explains why ρ -EOS consistently achieves competitive or superior accuracy with reduced runtime across all initial length settings.

Ablation on ρ thresholds $[\rho_{\text{low}}, \rho_{\text{high}}]$. We further investigate the sensitivity of ρ -EOS to the choice of the density thresholds $[\rho_{\text{low}}, \rho_{\text{high}}]$. As shown in Table 5, Sym (i.e., symmetrically setting ρ_{low} and ρ_{high} thresholds at intervals of 0.1) varying the thresholds over a wide range leads to only minor fluctuations in accuracy and runtime, indicating low sensitivity to precise threshold tuning. Across different threshold configurations, ρ -EOS consistently maintains stable accuracy while exhibiting predictable trade-offs between effective token ratio and total token count. In particular, wider length-equilibrium regions (e.g., $[0.2, 0.8]$) favor conservative length adjustment, resulting in higher E_{ratio} but slightly reduced E_{token} and T_{runtime} . Conversely, narrower or asymmetric settings allow more aggressive adjustment,

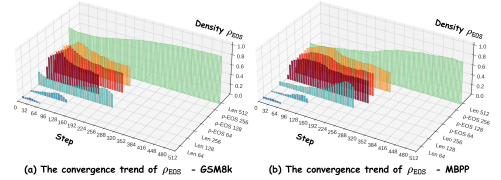
Table 6. Comparison on EOS Density (ρ) and Confidence for Length Control and Single Stage vs. Two Stage. Ablations are conducted on GSM8K and MBPP with LLaDA-Instruct-8B, $L_{\text{init}} = 64$.

| Metric | GSM8k | | | | MBPP | | | |
|----------------------|--------------|--------------------|-------------|--------------------|--------------|--------------------|------------|--------------------|
| | Single Stage | | Two Stage | | Single Stage | | Two Stage | |
| | Confidence | Density (ρ) | Confidence | Density (ρ) | Confidence | Density (ρ) | Confidence | Density (ρ) |
| A_{acc} | 73.7 | 84.2 | 84.6 | 84.4 | 40.0 | 40.6 | 38.2 | 40.4 |
| E_{token} | 224.3 | 252.2 | 246.0 | 219.9 | 340.7 | 335.9 | 321.8 | 335.3 |
| N_{token} | 256.6 | 361.0 | 331.0 | 414.9 | 546.5 | 594.4 | 587.1 | 602.3 |
| E_{ratio} | 87.4% | 70.0% | 74.5% | 53.0% | 62.3% | 55.5% | 54.8% | 55.7% |
| T_{runtime} | 888 | 823 | 1090 | 1049 | 2560 | 2030 | 4124 | 2030 |

increasing E_{token} at the cost of additional denoising steps. This robustness suggests that the **implicit EOS density provides a reliable and well-calibrated signal of length sufficiency**, making ρ -EOS resilient to moderate variations in hyper-parameter choices. Moreover, the asymmetric threshold pair [0.4, 0.8] reach a peak performance when $L_{\text{init}}=64$. We attribute this to the fact that the current model starts from a shorter initial length of 64, so a prior, the model tends to become longer, requiring a loose lower bound and a tight upper bound. Of course, we also found in the experiment of longer initial lengths, they do not have this prior knowledge, so they may not need this asymmetric boundary.

Ablation to the expansion factor function $E_{\text{factor}}(\cdot)$. Table 5 compares different selection of the expansion factor function $E_{\text{factor}}(\cdot)$. The constant expansion strategy in DAEDAL, improves over the baseline but remains limited in its responsiveness to large length mismatches. In contrast, the linear expansion function adjusts the expansion magnitude proportionally to the deviation of ρ_{EOS} from the length-equilibrium region, enabling faster correction when the current length is moderately misaligned. The exponential expansion function further amplifies this effect. When ρ_{EOS} is extremely low or high, the strategy applies substantially stronger length adjustments, allowing it to rapidly reach a stable denoising regime. As evidenced by the higher accuracy and few average adjustment steps in Table 5, these results confirm that **adapting the adjustment magnitude to the confidence of the length signal is crucial**, and that aggressive correction in early stages can significantly accelerate convergence without sacrificing accuracy.

Comparison on Using Confidence and Density of EOS as Length Control Signal and Single Stage vs. Two Stage. Table 6 compares using EOS confidence versus EOS density (ρ) as the length control signal, under both single-stage and two-stage length adjustment strategies. Across both GSM8K and MBPP, ρ -EOS **almost consistently outperforms confidence-based control**. In the single-stage setting, confidence-based signals suffer from instability, leading to suboptimal accuracy and inefficient length adjustment. As mentioned in Yang et al. (Yang et al., 2025a), masked dLLMs face EOS Trap during early decoding phase, and the confidence of EOS is significantly higher than that of other non-EOS. Therefore, this may lead to inaccurate length



Impact Statement

This paper presents work whose goal is to advance the field of Machine Learning. There are many potential societal consequences of our work, none which we feel must be specifically highlighted here.

References

- Achiam, J., Adler, S., Agarwal, S., Ahmad, L., Akkaya, I., Aleman, F. L., Almeida, D., Altenschmidt, J., Altman, S., Anadkat, S., et al. Gpt-4 technical report. *arXiv preprint arXiv:2303.08774*, 2023.
- Anthropic, C. . System card: Claude sonnet 4.5, 2025a. URL <https://www.anthropic.com/claude-sonnet-4-5-system-card>.
- Anthropic, C. . System card: Claude opus 4 & claude sonnet 4, 2025b. URL <https://www.anthropic.com/claude-4-system-card>.
- Arriola, M., Gokaslan, A., Chiu, J. T., Yang, Z., Qi, Z., Han, J., Sahoo, S. S., and Kuleshov, V. Block diffusion: Interpolating between autoregressive and diffusion language models. *arXiv preprint arXiv:2503.09573*, 2025.
- Austin, J., Johnson, D. D., Ho, J., Tarlow, D., and Van Den Berg, R. Structured denoising diffusion models in discrete state-spaces. *Advances in neural information processing systems*, 34:17981–17993, 2021a.
- Austin, J., Odena, A., Nye, M., Bosma, M., Michalewski, H., Dohan, D., Jiang, E., Cai, C., Terry, M., Le, Q., et al. Program synthesis with large language models. *arXiv preprint arXiv:2108.07732*, 2021b.
- Bai, J., Bai, S., Chu, Y., Cui, Z., Dang, K., Deng, X., Fan, Y., Ge, W., Han, Y., Huang, F., et al. Qwen technical report. *arXiv preprint arXiv:2309.16609*, 2023.
- Brown, T., Mann, B., Ryder, N., Subbiah, M., Kaplan, J. D., Dhariwal, P., Neelakantan, A., Shyam, P., Sastry, G., Askell, A., et al. Language models are few-shot learners. *Advances in neural information processing systems*, 33: 1877–1901, 2020.
- Chen, M., Tworek, J., Jun, H., Yuan, Q., Pinto, H. P. D. O., Kaplan, J., Edwards, H., Burda, Y., Joseph, N., Brockman, G., et al. Evaluating large language models trained on code. *arXiv preprint arXiv:2107.03374*, 2021.
- Cheng, S., Bian, Y., Liu, D., Zhang, L., Yao, Q., Tian, Z., Wang, W., Guo, Q., Chen, K., Qi, B., et al. Sdar: A synergistic diffusion-autoregression paradigm for scalable sequence generation. *arXiv preprint arXiv:2510.06303*, 2025.
- Cobbe, K., Kosaraju, V., Bavarian, M., Chen, M., Jun, H., Kaiser, L., Plappert, M., Tworek, J., Hilton, J., Nakano, R., et al. Training verifiers to solve math word problems, 2021. URL <https://arxiv.org/abs/2110.14168>, 9, 2021.
- DeepMind. Gemini diffusion, 2025. URL <https://deepmind.google/models/gemini-diffusion/>.
- Gong, S., Li, M., Feng, J., Wu, Z., and Kong, L. Diffuseq: Sequence to sequence text generation with diffusion models. *arXiv preprint arXiv:2210.08933*, 2022.
- Gong, S., Agarwal, S., Zhang, Y., Ye, J., Zheng, L., Li, M., An, C., Zhao, P., Bi, W., Han, J., et al. Scaling diffusion language models via adaptation from autoregressive models. *arXiv preprint arXiv:2410.17891*, 2024.
- Gong, S., Zhang, R., Zheng, H., Gu, J., Jaitly, N., Kong, L., and Zhang, Y. Diffucoder: Understanding and improving masked diffusion models for code generation. *arXiv preprint arXiv:2506.20639*, 2025.
- He, Z., Sun, T., Tang, Q., Wang, K., Huang, X.-J., and Qiu, X. Diffusionbert: Improving generative masked language models with diffusion models. In *Proceedings of the 61st annual meeting of the association for computational linguistics (volume 1: Long papers)*, pp. 4521–4534, 2023.
- Khanna, S., Kharbanda, S., Li, S., Varma, H., Wang, E., Birnbaum, S., Luo, Z., Miraoui, Y., Palrecha, A., Ermon, S., et al. Mercury: Ultra-fast language models based on diffusion. *arXiv preprint arXiv:2506.17298*, 2025.
- Kim, J., Cheuk-Kit, L., Domingo-Enrich, C., Du, Y., Kakade, S., Ngotiaoco, T., Chen, S., and Albergo, M. Any-order flexible length masked diffusion. *arXiv preprint arXiv:2509.01025*, 2025.
- Li, J., Dong, X., Zang, Y., Cao, Y., Wang, J., and Lin, D. Beyond fixed: Training-free variable-length denoising for diffusion large language models. *arXiv preprint arXiv:2508.00819*, 2025.
- Lightman, H., Kosaraju, V., Burda, Y., Edwards, H., Baker, B., Lee, T., Leike, J., Schulman, J., Sutskever, I., and Cobbe, K. Let’s verify step by step. In *The Twelfth International Conference on Learning Representations*, 2023.
- Liu, A., He, M., Zeng, S., Zhang, S., Zhang, L., Wu, C., Jia, W., Liu, Y., Zhou, X., and Zhou, J. Wedlm: Reconciling diffusion language models with standard causal attention for fast inference. *arXiv preprint arXiv:2512.22737*, 2025.
- Lou, A., Meng, C., and Ermon, S. Discrete diffusion modeling by estimating the ratios of the data distribution. *arXiv preprint arXiv:2310.16834*, 2023.

-
- Muennighoff, N., Yang, Z., Shi, W., Li, X. L., Fei-Fei, L., Hajishirzi, H., Zettlemoyer, L., Liang, P., Candès, E., and Hashimoto, T. s1: Simple test-time scaling. *arXiv preprint arXiv:2501.19393*, 2025.
- Nie, S., Zhu, F., You, Z., Zhang, X., Ou, J., Hu, J., Zhou, J., Lin, Y., Wen, J.-R., and Li, C. Large language diffusion models. *arXiv preprint arXiv:2502.09992*, 2025.
- Sahoo, S., Arriola, M., Schiff, Y., Gokaslan, A., Marroquin, E., Chiu, J., Rush, A., and Kuleshov, V. Simple and effective masked diffusion language models. *Advances in Neural Information Processing Systems*, 37:130136–130184, 2024.
- Song, Y., Zhang, Z., Luo, C., Gao, P., Xia, F., Luo, H., Li, Z., Yang, Y., Yu, H., Qu, X., et al. Seed diffusion: A large-scale diffusion language model with high-speed inference. *arXiv preprint arXiv:2508.02193*, 2025.
- Touvron, H., Lavril, T., Izacard, G., Martinet, X., Lachaux, M.-A., Lacroix, T., Rozière, B., Goyal, N., Hambro, E., Azhar, F., et al. Llama: Open and efficient foundation language models. *ArXiv preprint*, abs/2302.13971, 2023. URL <https://arxiv.org/abs/2302.13971>.
- Wang, C., Rashidinejad, P., Su, D., Jiang, S., Wang, S., Zhao, S., Zhou, C., Shen, S. Z., Chen, F., Jaakkola, T., et al. Spg: Sandwiched policy gradient for masked diffusion language models. *arXiv preprint arXiv:2510.09541*, 2025.
- Wu, Z., Zheng, L., Xie, Z., Ye, J., Gao, J., Feng, Y., Li, Z., W., V., Zhou, G., and Kong, L. Dreamon: Diffusion language models for code infilling beyond fixed-size canvas, 2025. URL <https://hkunlp.github.io/blog/2025/dreamon>.
- Yang, J., Chen, G., Hu, X., and Shao, J. Taming masked diffusion language models via consistency trajectory reinforcement learning with fewer decoding step. *arXiv preprint arXiv:2509.23924*, 2025a.
- Yang, Y., Wang, C., Wang, S., Wen, Z., Qi, B., Xu, H., and Zhang, L. Diffusion llm with native variable generation lengths: Let [eos] lead the way. *arXiv preprint arXiv:2510.24605*, 2025b.
- Ye, J., Xie, Z., Zheng, L., Gao, J., Wu, Z., Jiang, X., Li, Z., and Kong, L. Dream 7b, 2025. URL <https://hkunlp.github.io/blog/2025/dream>.
- Zhao, S., Gupta, D., Zheng, Q., and Grover, A. d1: Scaling reasoning in diffusion large language models via reinforcement learning. *arXiv preprint arXiv:2504.12216*, 2025.
- Zheng, K., Chen, Y., Mao, H., Liu, M.-Y., Zhu, J., and Zhang, Q. Masked diffusion models are secretly time-agnostic masked models and exploit inaccurate categorical sampling. *arXiv preprint arXiv:2409.02908*, 2024.
- Zhu, F., Wang, R., Nie, S., Zhang, X., Wu, C., Hu, J., Zhou, J., Chen, J., Lin, Y., Wen, J.-R., et al. Llada 1.5: Variance-reduced preference optimization for large language diffusion models. *arXiv preprint arXiv:2505.19223*, 2025a.
- Zhu, F., You, Z., Xing, Y., Huang, Z., Liu, L., Zhuang, Y., Lu, G., Wang, K., Wang, X., Wei, L., et al. Llada-moe: A sparse moe diffusion language model. *arXiv preprint arXiv:2509.24389*, 2025b.

A. Appendix

A.1. Why does ρ -EOS work? – Implicit length awareness in masked dLLMs by treating padding EOS as a part of response.

At the core of ρ -EOS lies a simple but critical hypothesis: *masked diffusion language models implicitly estimate how much generation space they need for a given input, even before the sequence is fully denoised*. Importantly, this behavior is not an emergent artifact of our inference strategy, but is deeply rooted in the training engineering implementation of masked dLLMs. In masked diffusion large language models such as LLaDA (Nie et al., 2025), padding EOS tokens are explicitly treated as part of the response sequence and are randomly masked during training. As a result, the model is repeatedly trained to jointly predict semantic tokens and EOS tokens under partial observation. This training paradigm forces the model to reason not only about *what* content should be generated, but also *where* meaningful content should end. Consequently, the prediction of EOS becomes intrinsically coupled with the model’s internal estimate of length sufficiency.

Crucially, this latent estimate is not exposed as an explicit scalar length prediction. Instead, it manifests implicitly through property of special functional token—the density of EOS over the remaining masked positions. From a denoising perspective, when the model assigns high probability mass to EOS at masked locations, it signals that the semantic content is largely complete and that the remaining generation space is redundant. Conversely, a consistently low implicit EOS density indicates that the model still requires additional capacity to express the intended response, and is therefore reluctant to terminate. Viewed from this angle, ρ -EOS does not introduce an external heuristic for length control. Instead, it *reads out* and *amplifies* a signal that the model has already learned to encode during training. By monitoring the implicit EOS density and feeding it back into the denoising process, our method aligns inference-time length adaptation with the model’s internal notion of response completeness.

This close alignment between training and inference is a key reason why ρ -EOS enables stable and effective bidirectional length control without additional supervision or multi-stage procedures. *In essence, variable-length inference emerges naturally when the inference process respects the semantics of EOS prediction learned by masked diffusion large language models.*

A.2. Why does implicit EOS density ρ outperform EOS confidence for single-stage length control? – A side effect of treating padding EOS as part of the response.

While treating padding EOS tokens as part of the response endows masked diffusion language models with implicit length awareness, it also introduces a non-trivial side effect that overconfidence on EOS may lead to instability in using it as a single-stage length control signal.

In particular, as observed in Yang et al. (Yang et al., 2025a), masked dLLMs often exhibit an EOS Trap phenomenon: during early denoising steps, the predicted confidence of EOS is significantly higher than that of non-EOS ones. This behavior is a direct consequence of the training paradigm. Since padding EOS tokens may occupy a large fraction of the sequence during training and are randomly masked, the model is frequently optimized to recover EOS under high uncertainty. As a result, in early decoding steps—when most positions remain masked and semantic structure has not yet emerged—the model tends to assign disproportionately high probability mass to EOS. Importantly, this high EOS confidence does not indicate semantic completeness, but rather reflects the model’s uncertainty and its bias toward the statistically termination token.

When EOS confidence is directly used as a length control signal, this early-stage overconfidence can prematurely trigger contraction or suppress necessary expansion. Such misaligned length decisions are particularly harmful in a single-stage setting, where length adjustment and semantic denoising are tightly interleaved. This explains the performance degradation observed when EOS confidence is employed as the control signal for single-stage strategy. In contrast, the implicit EOS density ρ aggregates EOS mass over all remaining masked positions, providing a global and temporally smoother estimate of length sufficiency. Therefore, implicit density ρ serves as a more robust length control signal than confidence.